Influence of Cation on Charge Recombination in Dye-Sensitized TiO_2 Electrodes

Carol L. Olson*,†

Department of Physics, Imperial College, Blackett Laboratory, Prince Consort Road, London SW7 2BZ, United Kingdom

Received: December 19, 2005; In Final Form: March 1, 2006

The reaction of a dye cation recombining with an electron in TiO_2, in the presence of Li^+, Ca^{2+}, and TBA^+ cations, was studied with laser-induced transient absorption measurements. The active cations, Li^+ and Ca^{2+}, shorten the dye cation lifetime on sensitized TiO_2 but not ZnO electrodes. By combining the absorbance measurements of the dye cation with simultaneous measurements of the current transient, the contribution of the recombination reaction to the current is identified. Furthermore, classical porous electrode theory is used to quantify the behavior of the heterogeneous electrode, and in doing so, the processes contributing to photoinduced current are identified as Helmholtz layer charging, porous electrode charging, recombination reactions, and surface diffusion of the active cations. The rate of charge recombination is proportional to the concentration of initially deposited active cations. The effect of water on the recombination rate and the current is also observed.

Introduction

With demonstrated efficiencies of about 10%, dye-sensitized solar cells have stimulated recent interest in molecular approaches to solar energy conversion.[1−3] In these photoelectrochemical devices, a wide band-gap transition metal oxide electrode is sensitized to visible light with the adsorption of a molecular dye on its surface. The high efficiency is due to the large difference in the interfacial electron-transfer rate associated with injection from the dye into the oxide, which is on the order of $>10^{-12}$ s, and that associated with recombination of the dye cation with an electron from the oxides, on the order of 10^{-6} s.[4−13]

The electron-transfer events in a dye-sensitized solar cell are summarized in the schematic representation shown in Figure 1. The excited dye injects an electron, at a rate k_I, occurring within picoseconds, into the conduction band of the TiO_2. If it does not recombine, at a rate of k_{R1}, with a dye cation, then it will travel out to the outer circuit to perform work. An iodide/triiodide redox couple in the electrolyte regenerates the dye cation to its charge neutral state, with a rate $k_{redox} > k_{R1}$, and transports the resulting positive charge to the counter electrode. To observe the recombination reaction of the dye cation with an electron from the TiO_2, a nonredox-active electrolyte is used. Electron injection might also be foiled if the dye's excited-state decays, at a rate k_{R2}, before injection occurs. However, studies of different dyes with different photophysics and with ground and excited states differing by up to 600 mV have shown that the rate of excited-state decay does not make an important contribution to the electron injection or the charge recombination kinetics.[10,12,14,15]

Understanding electron injection (k_I) and charge recombination (k_{R1}) continue to be a key to optimizing these solar cells. Difficulties have emerged, however, because different models for charge recombination have been proposed. In a recent review, the transport through the mesoporous films was described as "not well understood", possibly due to surface states and/or screening by the electrolyte.[16] The heterogeneity associated with the nanocrystalline electrode has been a stumbling block. Also, polarization occurs in the TiO_2 electrode, which is clearly influenced by the presence of active cations in the electrolyte. The evidence presented in this paper shows that cations, such as Li^+ and Ca^{2+}, which interact with the TiO_2 surface, influence the rate of charge recombination. Furthermore, by application of classical electrode theory, the heterogeneity of the porous electrode may be quantified, and the processes contributing to the photocurrent may be identified.

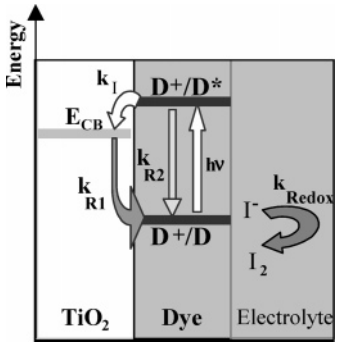

Figure 1. Schematic representation of the charge-transfer processes in the dye-sensitized solar cell. k_I is the electron injection rate, k_{redox} is the redox reaction rate, and k_{R1} and k_{R2} are the rates of the recombination reaction and the excited-state decay.

Experimental Methods

Sample Preparation. TiO_2 films were prepared by doctor-blading the colloidal solutions onto a (TEC-15) fluorine-doped SnO_2 conducting glass microscope slide (Hartford glass) using Scotch Magic Tape as spacers placed 1 cm apart as described previously.[2] The thickness of the sintered films was measured using a step profilometer, a Dektak IIA Surface Profile

* Author to whom correspondence should be addressed. E-mail: carol.olson@fotomol.uu.se.

† Present address: Department of Physical Chemistry, Uppsala University, Uppsala, Sweden.

10.1021/jp057383d CCC: $33.50
Published on Web 04/20/2006

Measuring System (Sloan Technology). The films used in this work were mainly 8 μm films made with two layers of scotch tape. The air-dried films were sintered at 450 °C for 20 min. ZnO films, 4 μm in thickness, had been prepared as described previously.[17]

For dye sensitization, when the 8 μm films cooled to ~70 °C, they were immersed in room-temperature ethanolic dye solutions and kept there overnight. TiO_2 films were sensitized with $RuL_2(NCS)_2$,[9] (also known as N719), where L is 4,4′-dicarboxy-2,2′-bipyridyl. ZnO films were sensitized with Ru(HP-terpy)(Me_2-bpy) NCS,[18] (also known as Z105), which was dissolved in 70:30 ethanol/dimethyl sulfoxide (DMSO) solution at 10^{-4} M. The Ru(HP-terpy)(Me_2-bpy) NCS dye, which binds to the ZnO surface through a phosphonate group, was selected to avoid problems with the instability of the carboxylated dyes on the ZnO electrode as reported previously.[17,19] After sensitization, the films were immediately covered with a 1:1 ethylene carbonate/propylene carbonate solution and thin cover glasses and stored under dark, dry conditions to avoid dye degradation.

Dry acetonitrile was used as the solvent in all experiments. Acetonitrile was stirred overnight with calcium hydride to remove water. The neat dry acetonitrile was then separated from the solution by distillation under an argon atmosphere. Tetrabutlyammonium perchlorate (TBAP), $LiClO_4$, and $Ca(ClO_4)_2$ were dried under vacuum. The water content of the electrolytes was measured with a Karl Fisher apparatus (Metrohm 737 Coulometer). Pure distilled water was added as indicated.

The electrochemistry was performed in a three-electrode cell with a mesh platinum counter electrode and a silver−silver chloride reference electrode. Applied potentials are dropped between the working and the reference electrodes and are relative to the Ag/AgCl reference electrode. Argon was bubbled through the electrolyte to minimize exposure of the system to oxygen. The active window area of the three-electrode cell was quartz.

Transient Absorption Spectroscopy. Nanosecond to millisecond transient absorption spectroscopy was performed as described previously.[9] When time-resolved current measurements were taken, they were taken simultaneously with the absorption measurements. A sensitized film with a macroscopic area of 1 cm^2 was placed in a three-electrode cell, with the sample as the working electrode, a platinum mesh counter electrode, and a Ag/AgCl reference electrode.

A nitrogen laser-pumped dye laser generated ~510 nm excitation pulses (~0.1 mJ/cm^2) at ~0.9 Hz. The absorption difference was measured using a 100 W tungsten probe lamp guided through two 20 nm bandwidth monochromators with the sample between them. The absorption data were collected with a photodiode, filtered with appropriate high-band or low-band filters, and digitized with a standard oscilloscope (TDS-220 Tektronics DSO). A potentiostat connected to the three-electrode cell allowed a bias to be applied and also transmitted the current to a second channel on the oscilloscope.

The excitation wavelength was chosen near the maximum ground-state absorption of the dye, and the optical density of the sample was kept low, between 0.3 and 0.6, to avoid the nonlinear effects cited by previous researchers.[4] Figure 2 shows the spectra of excited dye cations on sensitized TiO_2 and ZnO films ~2 μs after excitation and electron injection. The maximum for N719 dye cations occurs at 800 nm, but the maximum for Z105 occurs at 725 nm, and these were the probe wavelengths for the respective materials.

The data were collected as follows: Immediately after the bias was applied, the transient absorption data for the interval between 0.2 and 22.5 μs were gathered and averaged by the oscilloscope for either 16 or 32 laser pulses and recorded. Then the current for this interval was recorded. The transient absorption and current data were collected in this way for time intervals from 2 to 450 μs, 20 μs to 4.5 ms, 200 μs to 45 ms, and 2 ms to 0.5 s. Optical scans were averaged over 16−32 pulses, but current data were not averaged but collected after the last optical scan. It would take 3−5 min to complete a data set at any given bias, and then the data at the next bias would be taken and so on.

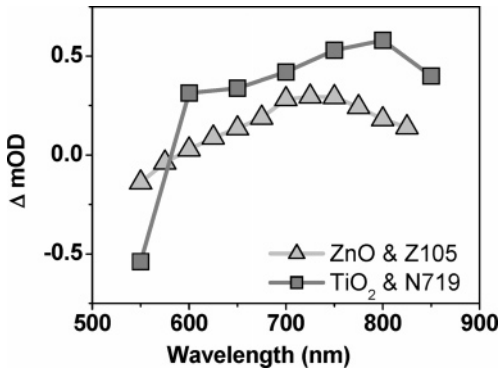

Figure 2. Transient absorption spectra for ZnO films sensitized with Z105 dye (▲) and TiO_2 films sensitized with N719 dye (■), taken 2 μs after excitation at 510 nm. Films were prepared with the same initial optical density.

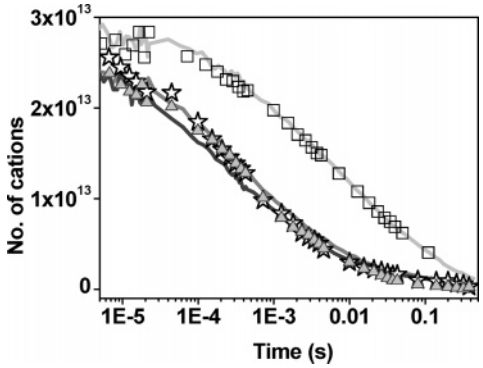

Figure 3. Decay of the N719 dye cation on TiO_2 exposed to the following electrolytes: 0.1 M TBAP in MeCN (at 0 V, light gray line; at no bias, □); 0.1 M $LiClO_4$ and 0.1 M TBAP in MeCN (at 0 V, gray line; at no bias, ▲); 0.1 M $Ca(ClO_4)_2$ in MeCN (at 0 V, black line; at no applied bias, ☆).

To minimize desorption and/or degradation of the dye caused by negative applied biases, −700 mV was the negative limit to the applied potentials. Data were collected at zero applied potential before and after all experiments to monitor the effect of the experiment on the dye.

The reported numbers of cations were calculated using the Beer−Lambert law from the concentration in mol cm^{-3} for a film volume of 1 cm^2 in area and 8×10^{-4} cm in thickness. The extinction coefficient for the N719 dye cation was taken to be 12 000 M^{-1} cm^{-1}.[8]

Results and Discussion

No Applied Bias. The dye cation lifetime is shortened in the presence of Li^+ or Ca^{2+} ions, as shown in Figure 3. They will be referred to as "active" ions and distinguished from TBA^+, which acts as an inert supporting electrolyte. Figure 3 also shows that the behaviors at no applied bias and at an applied bias of 0 mV are the same and that Ca^{2+} and Li^+ ions, in the

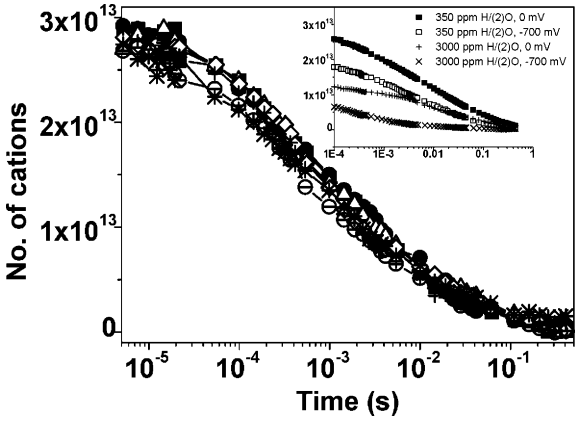

Figure 4. Applied biases of 0 mV (■), −100 mV (●), −200 mV (△), −300 mV (◇), −400 mV (∗), −500 mV (+), and −600 mV (⊖) have no effect on the cation decay of a sensitized TiO_2 film in MeCN with TBAP as the supporting electrolyte. Inset: The cation lifetime does show a bias dependence when water is present.

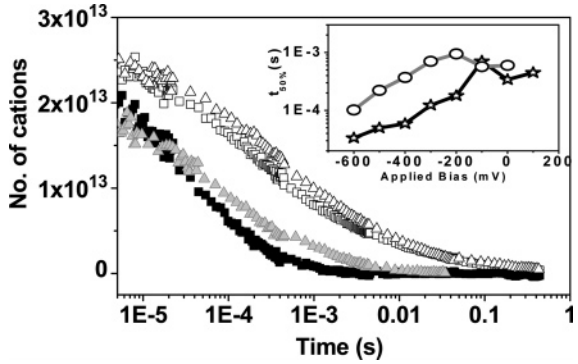

Figure 5. Dye cation decays for sensitized TiO_2: at 0 mV in 0.1 M $Ca(ClO_4)_2$ with 260 ppm H_2O (□); at −600 mV in 0.1 M $Ca(ClO_4)_2$ with 260 ppm H_2O (■); at 0 mV in 0.1 M $LiClO_4$ and 0.1 M TBAP with 300 ppm H_2O (△); at −600 mV in 0.1 M $LiClO_4$ and 0.1 M TBAP with 300 ppm H_2O (▲). Inset: Decay half-life, $t_{50\%}$, as a function of bias for "dry" electrolytes containing Ca^{2+} (☆) and Li^+ (○) ions.

absence of an applied bias, produce the same decays within experimental error.

With Applied Bias. Figure 4 demonstrates that the application of biases from 0 to −600 mV does not change the recombination kinetics of sensitized films in "dry" acetonitrile (i.e., ≤300 ppm water), with TBAP as the supporting electrolyte. The electrolyte contained only 120 ppm H_2O, not enough to affect the behavior under bias. The inset shows that a bias dependence is found at water concentrations of 350 and 3000 ppm (see below).

In the presence of Li^+ or Ca^{2+} ions, however, the dye cation−electron recombination process accelerates with a negative applied bias. Figure 5 compares the dye cation decays of sensitized TiO_2 exposed to Li^+ or Ca^{2+} ions at two different applied biases. The Ca^{2+} decay curve has a slightly different shape from that of Li^+, but the overall effect of an applied bias, in speeding up the decay of the cation signal, is the same in both cases. The inset in Figure 5 compares the cation decay half-life ($t_{50\%}$) for the Li^+ or Ca^{2+} systems as a function of applied bias. In the presence of Li^+ or Ca^{2+} ions, the recombination kinetics accelerate at biases negative of −200 or −100 mV, respectively. This is consistent with the results of Haque et al.[8] The recombination rate is faster for the doubly charged Ca^{2+} ions, which suggests that the density of charge at the surface is a factor in the rate of the recombination reaction.

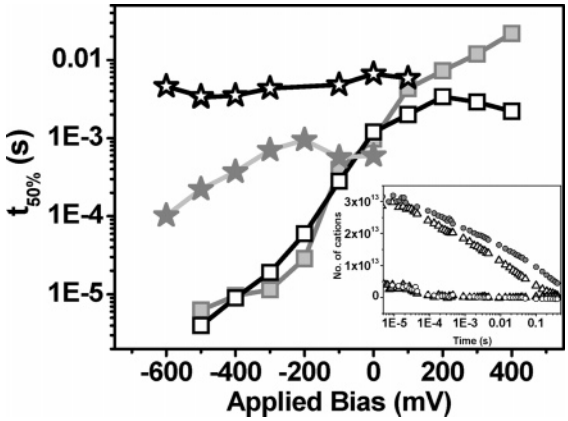

Figure 6. Cation decay half-life, $t_{50\%}$, over a range of applied biases for: TiO_2 films in MeCN with 0.1 M TBAP (☆) and with 0.1 M $LiClO_4$ (★); ZnO films in MeCN with 0.1 M TBAP (□) and with 0.1 M $LiClO_4$ (■). In sensitized ZnO films, the applied bias influences the cation lifetime, regardless of the presence of Li^+ ions, unlike TiO_2 films which show a bias dependence only with Li^+ ions, at potentials negative of −200 mV. Inset: Cation decays of sensitized ZnO films in MeCN at +300 mV with 0.1 M TBAP (△) and with 0.1 M $LiClO_4$ (●) and ZnO films in MeCN at −500 mV with 0.1 M TBAP (▲) and with 0.1 M $LiClO_4$ (○).

Figure 6 shows that the rate of charge recombination in ZnO is a function of applied bias, whether Li^+ ions are present or not. This is illustrated in the inset with decays of sensitized ZnO films, with and without Li^+ ions, at +300 and −500 mV. The dye cation lifetime of sensitized TiO_2, however, is influenced by applied bias, negative of −200 mV, only when Li^+ ions are present. The Li^+ ions change the oxidation state of the Ti^{4+} lattice ions to Ti^{3+}. This interaction populates the lowest energies in the conduction band, which then creates a surface dipole and lowers the work function.[20−25] The surface becomes more conductive, with electrons more available to recombine with dye cations. In ZnO, however, the transition metal oxidation state is not changed by the presence of the Li^+ ion, and the bias dependence in ZnO may be due to the increased surface conductivity that occurs when the material is reduced.[26]

Effect of Water on TiO_2 Films in Electrolytes with and without Active Cations. When water on the order of 10^3 ppm was added to the electrolytes, the initial concentration of dye cations was reduced irreversibly by roughly half due to desorption of the dye, as shown in the 3000 ppm data in the inset of Figure 4. Qu et al.[37] observed roughly a 50:50 mixture of carboxylate and carboxylic acid dye linkages on typical TiO_2 films and note that hydrolysis of the latter is well-known.

In the inert TBA^+ system with 300 ppm of water, the applied bias does not influence the dye cation lifetime, but a bias dependence is clearly seen with 3000 ppm of water, as shown in Figure 7 (left).

The recombination kinetics for systems with Li^+ and Ca^{2+} are affected differently in the presence of water, as shown in Figure 7 (right). In the case of Li^+, water hinders the acceleration of the kinetics between −300 and −600 mV. In the case of Ca^{2+}, water only delays the onset of the bias dependence from −100 to −200 mV. As lithium ions enter the TiO_2 lattice, the reduction of Ti^{4+} to Ti^{3+} sites is observed.[38] Augustsson et al have shown that Li insertion in anatase leads to an electron in the d-band, with significant electron correlation of the d-electrons in the Li_xTiO_2 system.[39] Therefore, Li^+ ion causes a charge-compensating neighboring electron to react with titania as would its own 2s electron. Li^+ cations prefer to interact with water rather than titania, forming a Li−OH hydroxide species

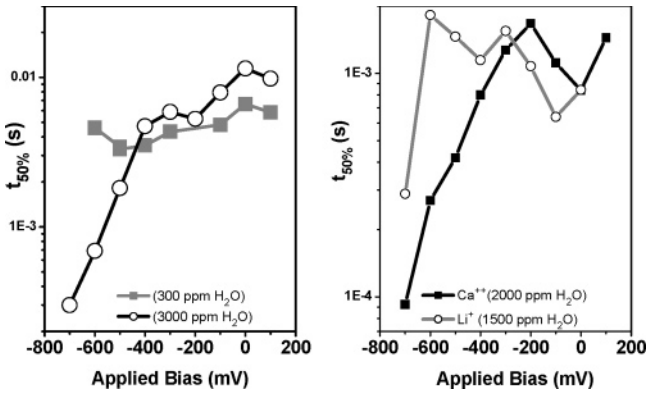

Figure 7. Left: Cation decay half-life ($t_{50\%}$) as a function of applied bias, for sensitized TiO_2 in inert electrolyte with 300 ppm H_2O (■) or 3000 ppm H_2O (○). Right: Cation decay half-life for 0.1 M $Ca(ClO_4)_2$ and 2000 ppm water (■) and for 0.1 M $LiClO_4$, 0.1 M TBAP, and 1500 ppm water (○).

at the surface, with additional water being adsorbed molecularly on top of this layer.[40] From metastable impact electron spectroscopy[40,41] and X-ray photoelectron spectroscopy[38] observations of hydrated titania, the Li 2s electron is involved in bonding water to a Li-precovered titania surface through the formation of a Li−OH species. It is the Li 2s electron that, in the absence of water, is transferred to the Ti^{3+} 3d and responsible for decreasing the titania work function.[42] Therefore, water inhibits the effect of Li^+ ions on titania. The increase in the current (data not shown), especially at applied biases more negative than −400 mV, with additional water suggests the occurrence of side reactions. Because it occurs in the TBAP and $Ca(ClO_4)_2$ systems, but not in the $LiClO_4$ system, it may be rationalized as the movement of holes to OH^- sites producing a hole current that enhances the electronic current. When Li^+ preferentially interacts with these OH^- sites then this process cannot happen.

Recombination Reaction Contribution to the Current. Measurements of the current were taken simultaneously with the absorbance measurements of the dye cations. To compare the current (the change in the number of electrons) with the number of cations, it is necessary to take the derivative of the cation decay curve (i.e., the change in the number of cations). The cation decays of sensitized TiO_2 in inert electrolyte (with 350 ppm H_2O, as shown in the inset to Figure 4) were fitted with polynomials, then differentiated and normalized, and are shown in Figure 8B. When the change in the number of cations has fallen to about 95% of its initial value, there is a noticeable change in the current, as is pointed out by the arrow in Figure 8. This shows that the contribution of the recombination reaction to the current ends at about 4.5×10^{-4} s and is superimposed upon another current process.

Porous Electrode Charging Due to Photoinjected Electrons. Suppose that the applied bias is 0 mV and the electrostatic changes to the material are caused by the photoinjected electrons. If the spatial distribution of photoinjected electrons follows Beer's law, then there is an exponential distribution of electrons across the film, with most of the electrons entering the TiO_2 from the side exposed to the light. This is analogous to a current pulse. It is relevant then to consider how a porous electrode in electrolyte responds to a current pulse.

The classical model of the porous electrode builds on the work of de Levie,[27] who considered the pores as uniform cylindrical channels of semi-infinite length, permeated with electrolyte. He modeled a section of a pore as the circuit model shown in Figure 9. When a constant voltage is applied to a

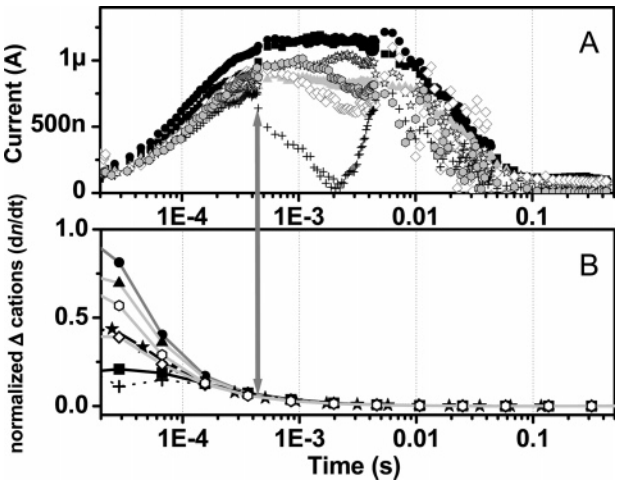

Figure 8. Data from simultaneous current and absorbance measurements: (A) photoinduced current from TiO_2 films with inert electrolyte (with 350 ppm H_2O) at different applied biases; (B) normalized derivative of cation decay curves (inset of Figure 4). The contribution of the charge recombination process to the current ends at about 0.45 ms; therefore another current process is also occurring. Applied biases: 0 mV (■), +100 mV (●), −100 mV (▲), −200 mV (★), −300 mV (◇), −400 mV (+), −500 mV (⬡).

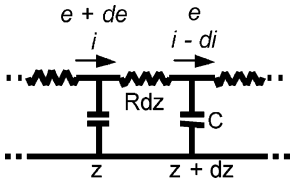

Figure 9. Equivalent circuit for a porous electrode. $E(z)$ is the potential (in V) as a function of spatial coordinate, z, $I(z,t)$ is the current (in A), R is the ohmic resistance of the pore per unit length (in Ω cm^{-1}), and C is the capacitance of the ionic double layer per unit pore length in the z-direction (in F cm^{-1}).

porous electrode, the voltage will travel through a transmission line arrangement of resistances and capacitances. He derived eq 1 for the charging of a porous electrode

$$\frac{\partial^2 e}{\partial z^2} - RC\frac{\partial e}{\partial t} = 0 \quad \text{and} \quad \frac{\partial^2 i}{\partial z^2} - RC\frac{\partial i}{\partial t} = 0 \qquad (1)$$

The current will show an Ohmic rise until the capacitive limit is reached, and then it will fall once the film is charged, producing the type of transient current shown in Figure 10, which shows the 0 mV curve from Figure 8.

Porous electrode charging behavior is found in the data. There are three features in the curve shown in Figure 10: (1) There is a broad peak from 10^{-5} to 0.1 s, (2) there is a small narrow peak at 2×10^{-5} s, and (3) there is a bite taken out of the broad peak from 2×10^{-5} to 4.5×10^{-4} s. The first feature is attributed to porous electrode charging, the second feature to Helmholtz layer charging, and the third to the recombination reaction. The rise in current here is complicated by the presence of the recombination reaction and Helmholtz layer charging. Figure 10 shows a fit to the current transient decay of the charging of a porous electrode.

Through the use of the model for a current pulse developed by Posey and Morozumi,[28] who solved eq 1 for various boundary conditions, the currents obtained with applied biases from +100 to −500 mV were fit with curves, as shown in Figure 11. Values for the resistance and the capacitance associated with the charging of a porous electrode could be extracted from these curves and were found to vary linearly

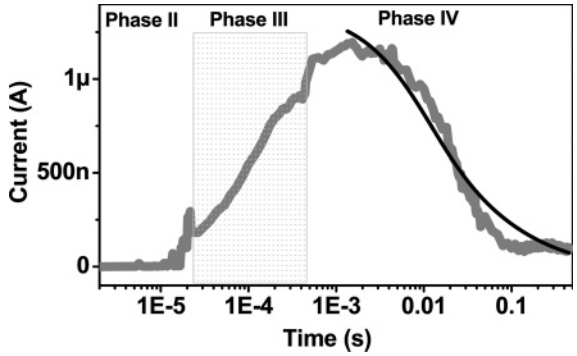

Figure 10. Schematic showing the phases of the photocurrent transient at 0 mV for sensitized TiO_2 in inert electrolyte with 350 ppm H_2O, (wide gray line), with current fit (black line) of the porous electrode charging decay, using the equivalent circuit for a porous electrode given in Figure 9. Phase I, electron injection, has already occurred at $t < 10^{-12}$ s. Phase II is the Helmholtz layer charging; phase III is the charge recombination reaction, superimposed upon porous electrode charging; phase IV is the decay of the porous electrode charging.

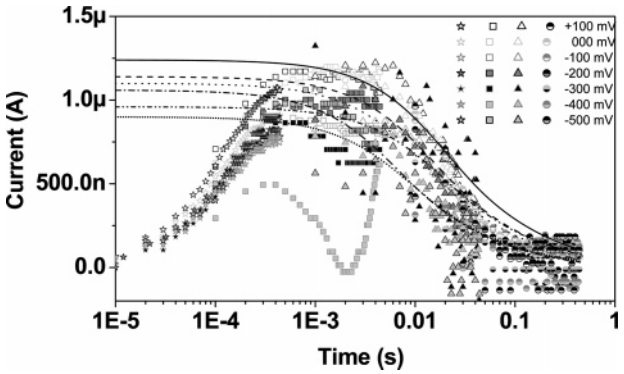

Figure 11. Composite curve of photocurrents of sensitized TiO_2 films in inert electrolyte (0.1 M TBAP) measured at four different time intervals (2 to 450 μs (stars), 20 μs to 4.5 ms (squares), 200 μs to 45 ms (triangles), and 2 ms to 0.5 s (circles)) at applied biases from +100 to −500 mV, with curve fits using porous electrode charging decays (0 mV (solid black line), −100 mV (dotted black line), −200 mV (solid gray line), −300 mV (dashed black line), −400 mV (dash−dotted black line), −500 mV (dashed gray line).

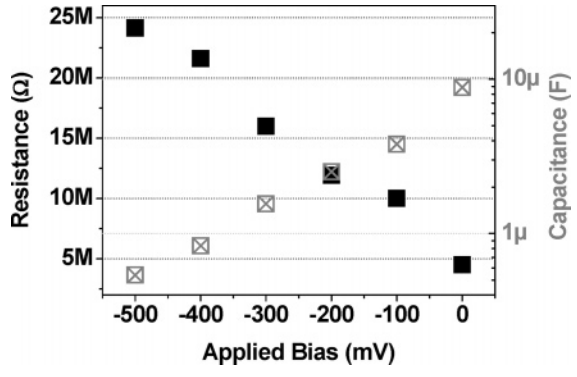

Figure 12. Capacitance (open squares with crosses) and resistance (■) values associated with porous electrode charging at different applied biases for a TiO_2 electrode in inert electrolyte (0.1 M TBAP in MeCN).

with applied bias as shown in Figure 12. The *RC* time constants were found to be in the range 13 s $\leq \tau \leq$ 40 s for applied biases from −500 to 0 mV. The trend in Figure 12 seems reasonable, however, because increasing resistance with more negative biases is consistent with the smaller currents observed at more negative biases in Figures 8 and 11.

This model describes well the data taken at 0 mV, but the data at more negative applied biases have features between 5 $\times 10^{-4}$ and 5 $\times 10^{-3}$ s that it does not account for. The current curves shown in Figure 8 are composites of different measurements taken in five different time regimes: 0.2 to 22.5 μs, 2 μs to 450 μs, 20 μs to 4.5 ms, 200 μs to 45 ms, and 2 ms to 0.5 s. These five datasets were merged, sorted, and averaged to produce the curves in Figure 8. Figure 11 shows the actual data from three time regimes: 2 to 450 μs, 20 μs to 4.5 ms, and 200 μs to 45 ms. At −400 and −500 mV, the data taken in the 20 μs time frame (squares) diverges from the next set of data in the 200 μs regime (triangles). These current measurements were taken at constant applied bias, but after 16−32 laser pulses needed to average the transient absorption data. Therefore, in actuality, the electrode is responding to waves of photoinjected electrons, which becomes more apparent at more negative applied biases. Only the charging of the porous electrode at constant bias due to a single current pulse, which describes the gross behavior of the current transient, is considered here, which lays the groundwork for future investigations of the detailed features between 5 $\times 10^{-4}$ and 5 $\times 10^{-5}$ s arising at more negative applied biases.

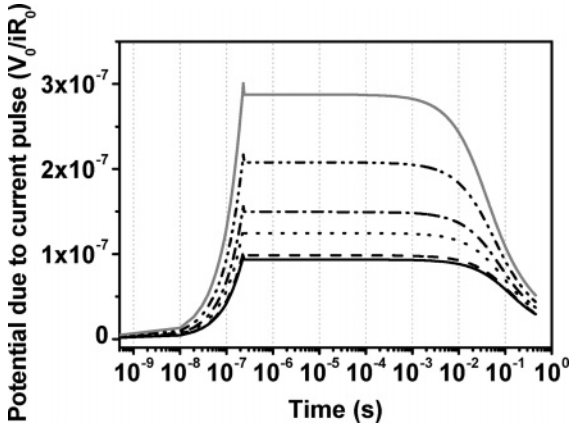

Figure 13. Potential experienced by a porous electrode due to a current pulse (on the side of the electrode nearest the pulse). The curves are calculated using a pulse duration of 2.2 $\times 10^{-7}$ s, and the *RC* time constants (τ) are extracted from the curve fits in Figure 11: $\tau = 40$ s (solid black line), $\tau = 38$ s (dashed black line), $\tau = 30$ s (dotted black line), $\tau = 25$ s (dash−dotted black line), $\tau = 18$ s (dash−dot−dotted black line), $\tau = 13$ s (solid gray).

Potential Due to Injected Electrons. The laser pulse has a duration of about 2 $\times 10^{-7}$ s. From the model of Posey and Morozumi,[28] a current pulse with a duration of about 200 ns produces, in a porous material with a relatively slow time constant (i.e., 13 s $\leq \tau \leq$ 40 s, see above), the potential curves shown in Figure 13. As the *RC* time constant of the material decreases, which occurs as the applied bias becomes more negative, the stronger the effective current pulse becomes.

Current Measurements in Electrolyte Containing Active Ions (Li^+ or Ca^{2+}). Figures 14 and 15 show the currents for sensitized TiO_2 in "dry" electrolytes with active ions, measured simultaneously with the cation decay curves shown in Figure 5. By comparison of these curves to the current in inert electrolyte, the broad features of these curves may be attributed to the processes of Helmholtz charging, porous electrode charging, recombination reactions, and interaction with the active ions.

Phases of the current transients from "dry" systems containing Ca^{2+} and Li^+ (at −400 mV) are indicated schematically, in Figure 16, compared to the current in inert electrolyte at 0 mV (from Figure 10). The −400 mV is typical of the data from −100 to −400 mV showing a clear peak due to the active cation, while −500 and −600 mV show a less distinguishable peak.

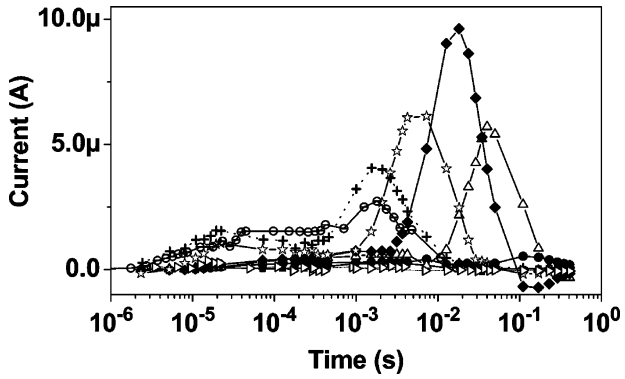

Figure 14. Currents for sensitized TiO_2 in 0.1 M $LiClO_4$, 0.1 M TBAP, and 300 ppm H_2O at applied biases of 0 mV, (■), −100 mV (●), −200 mV (△), −300 mV (◆), −400 mV (☆), −500 mV (+), −600 mV (⊖), and 0 mV (open right triangles). The two sets of data at 0 mV, taken before and after the data at other biases, are the same, showing that the system has not changed during the test.

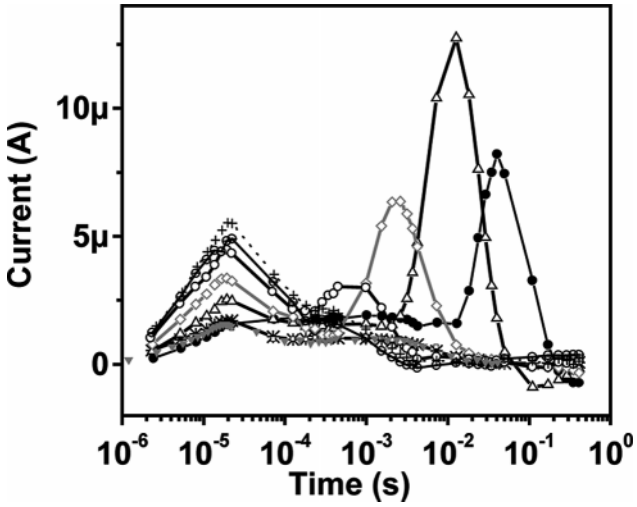

Figure 15. Currents for sensitized TiO_2 in 0.1 M $Ca(ClO_4)_2$ with 260 ppm H_2O at applied biases of +100 mV (∗), 0 mV, (□), −100 mV (●), −200 mV (△), −300 mV (◇), −400 mV (○), −500 mV (+), and −600 mV (⊖), with the final data set at 0 mV (solid right triangles) showing that the system has not changed during the experiment.

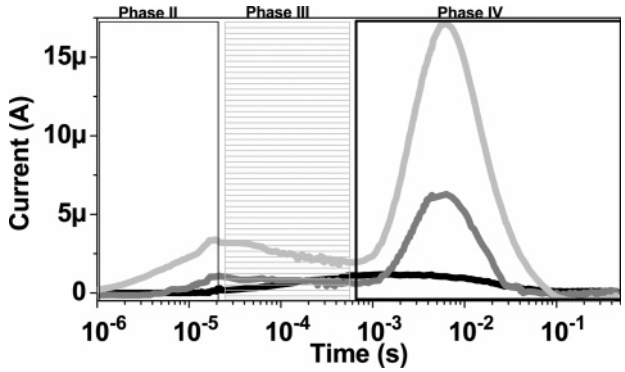

Figure 16. Schematic showing the phases occurring in current transients of sensitized TiO_2 electrodes in electrolytes with active ions, Li^+ at −400 mV (gray line) and Ca^{2+} at −400 mV (light gray line), as compared with the current transient in an inert electrolyte at 0 mV (black line).

Phase I, electron injection, has already occurred in times less than picoseconds. The earliest feature observed in the present data occurs in phase II, at 20 μs, and is attributed to Helmholtz layer charging. The charge recombination reaction occurs in phase III (20 μs to 0.5 ms) and is coupled with the porous electrode charging. Phase IV has a feature not seen in the inert electrolyte, an interaction with the active ion, which starts before the charging of the TiO_2 matrix has ended.

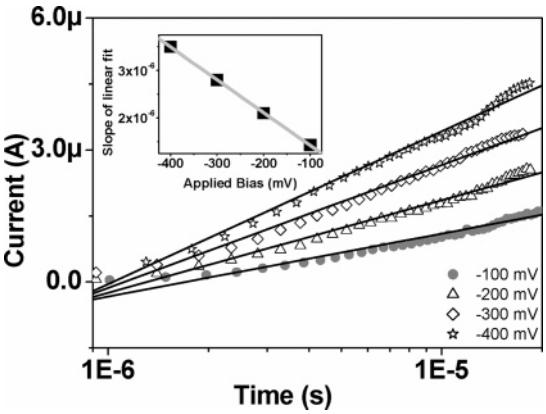

Figure 17. Linear fits to the data in Figure 15 showing Helmholtz layer charging in the Ca^{2+} system. Inset: Slopes of linear fits are proportional to applied bias, as expected for Helmholtz layer charging.

Helmholtz Layer Charging. A simple model for what is occurring in the first phase of the current is the following. If ions move through the electrolyte simply because of the electrostatic force of the applied potential, then the force on the ion should be proportional to the applied bias. The acceleration of the charge is the derivative of the current. So, if the slope of the current is proportional to the applied bias, then it is consistent with a current due to the electrostatic forces on ions. The current due to Helmholtz layer charging in the Ca^{2+} system is a linear function of bias as shown in Figure 17.

TBAP was not added to the $Ca(ClO_4)_2$ system to keep its ionic strength (0.25 M equiv^2) closer to the ionic strength of the $LiClO_4$/TBAP system (0.2 M equiv^2). However, it appears that the size difference and possible interaction between species in the TBA^+ and Li^+ ions complicates the Helmholtz layer charging in the Li^+ system. Therefore, this simple model cannot be applied to the Li^+ data. In the inert supporting electrolyte the Helmholtz layer charging current is visible but too small, compared to the noise, to fit.

Porous Electrode Charging in Electrolyte with Active Ions. While phase III in electrolytes containing Li^+ and Ca^{2+} is too convoluted to distinguish the porous electrode charging process, an important trend is clear in Figures 14 and 15. Unlike the currents in the inert electrolyte, these currents are increasing with more negative applied bias, suggesting that active ions lower the resistance of the TiO_2 with negative applied bias, which is consistent with equivalent circuit modeling of TiO_2 electrodes in Li^+-containing electrolyte. [29]

Interestingly, the bias dependence of the dye cation lifetime on sensitized TiO_2, in the presence of Li^+ ions, starts at −400 mV (see inset of Figure 5). Figure 14 shows that at this bias the Helmholtz layer charging produces a relatively large current and significantly overlaps with the porous electrode charging phase. This suggests that the currents associated with the Helmholtz layer charging at −400 and −500 mV are key in accelerating the dye cation lifetime.

Surface Diffusion of Active Ions. In the systems with active ions, the large current peaks are attributed to interaction with the ions because they were not seen in the inert electrolyte measurements. Solbrand et al.[30,31] previously used a diffusion model on photocurrent transients after about 5 ms taken in electrolytes with active ions at an applied bias of +300 mV. They did not identify the diffusion mechanism. Here, it is attributed to surface diffusion of the ions.

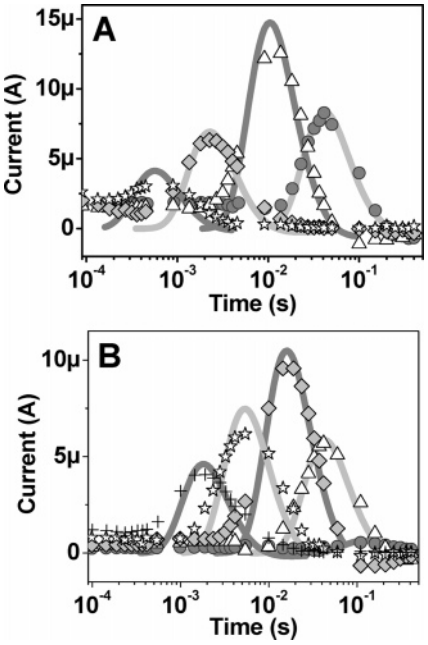

Figure 18. Details of Figures 14 and 15 showing ion surface diffusion curve fits for TiO_2 in (A) 0.1 M $Ca(ClO_4)_2$ or (B) 0.1 M $LiClO_4$ and 0.1 M TBAP at applied biases of −100 mV (●), −200 mV (△), −300 mV (◇), −400 mV (☆), and −500 mV (+). Curve fits are wide gray lines.

The diffusion process is considered here as the result of some amount of ions having been deposited at $t = 0$ and left to diffuse through the surface of the TiO_2 matrix. The diffusion equation is given in eq 2 where n is the electron concentration, D is the diffusion coefficient, t is time, and x is distance from the solid/electrolyte interface

$$\frac{\partial n}{\partial t} = D\frac{\partial^2 n}{\mathrm{d}x^2} \tag{2}$$

Equation 3 gives a well-known solution to this equation for surface diffusion in the xy-plane due to a line source along the y-axis in a semi-infinite solid, i.e., a solid bounded by the plane $x = 0$ and extending to infinity in the positive x direction[32]

$$n = \left(\frac{M}{2(\pi D)^{1/2}}\right)t^{-1/2}\exp(-x^2/4Dt) \tag{3}$$

In eq 3, M is the amount of diffusing substance deposited initially per unit length of the line source, t is time, x is the spatial coordinate, D is the surface diffusion coefficient, and n is the number of electrons. To compare this solution to the current ($\mathrm{d}n/\mathrm{d}t$), we can take the partial derivative with respect to time. Let c_1 and c_2 be constants where $c_1 = M/(4\pi D)^{1/2}$ and $c_2 = x^2/4D$, then the diffusion current becomes eq 4

$$i = c_1\exp\left(-\frac{c_2}{t}\right)\left(c_2 t^{-5/2} - \frac{1}{2}t^{-3/2}\right) \tag{4}$$

The solution to the diffusion equation as given in eq 4 was used to generate the curve fits shown in Figures 18A and 18B.

The initial amount of active ions deposited, M, (mol/cm) may be extracted from the curve fits in Figure 18. Figure 19 shows that the amount of ions initially deposited is directly proportional to the dye cation decay half-life, $t_{50\%}$. This suggests that the rate of the recombination reaction and the amount of ions adsorbed both directly depend on the local potential, (i.e., the overpotential) at the TiO_2/electrolyte interface. The literature[20,25,24,33−36] suggests that the amount of active ions adsorbed is equivalent to the number of delocalized electrons on surface five-coordinated Ti sites, populating the lowest conduction band energies. If this is so, then the recombination reaction has a first-order kinetic relationship with these surface electrons.

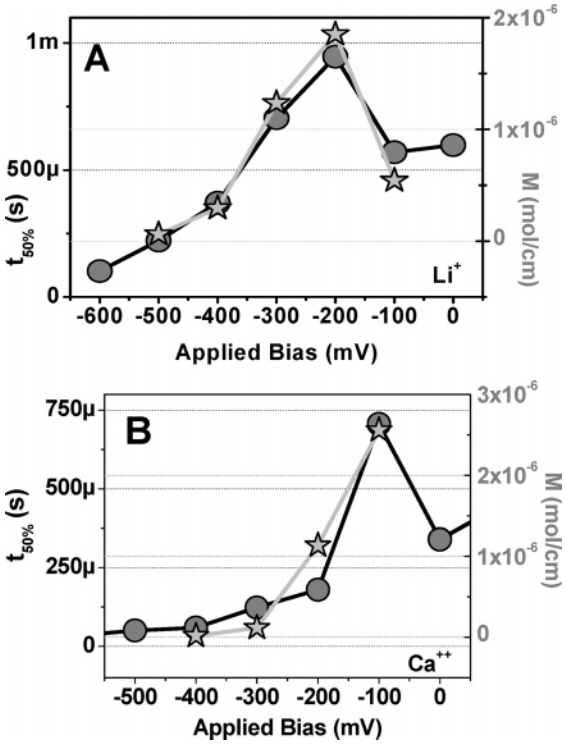

Figure 19. Initial amount of ions deposited, M (☆) extracted from the diffusion model curve fits of the ions, correlating with $t_{50\%}$ (○) of the recombination reaction with (A) Li^+ or (B) Ca^{2+} as active ions.

Reconciliation of Different Reports on Recombination Kinetics. Solbrand et al.[31] observed photocurrents that occurred later than the recombination reaction. They identified diffusion currents but did not explain the diffusion mechanism. They were really looking at phase IV, the surface diffusion of the ions.

Nelson[42] simulates the recombination process of an electron moving throughout a particle from trap to trap until it meets a dye cation and uses the statistical results of this simulation to model the recombination decay curves. The power law given in eq 5 is used with an exponential density of states for the electrons resulting in a stretched exponential, as given in eq 6. $t_{50\%}$ is the decay half-life, n is the "number of electrons per particle", α is a measure of the disorder in the system, and S is the cation concentration

$$t_{50\%} \propto n^{-1/\alpha} \tag{5}$$

$$S(t) = \mathrm{e}^{-(t/\tau)^{\alpha}} \tag{6}$$

The "number of electrons per particle", n, is derived from the change in optical density and quantifies the detected change in the number of Ti^{3+} sites per nanoparticle, i.e., the number of additional electrons in the d-orbitals. As a second independent measurement of n, they use the charge in the Helmholtz layer, which is achieved by integrating the current associated with Helmholtz layer charging. That these two measurements correlate supports the idea that most of the charge is at the surface. The modeling by Nelson[42] works because the quantity taken as the concentration of electrons, n in eq 5, is the excess charge associated with the double layer at a given applied potential.

The heterogeneity of the TiO_2 films is the reason cited by other researchers why there is a distribution of rate constants necessitating a sum of second-order[13,14] (or a sum of second- and first-order)[12] expressions to fit the cation decay curves. This heterogeneity can be quantified with classical porous electrode theory; it shows that a change in potential proceeds in a wave across a porous electrode, with the associated charging of pore segments. Therefore, any process occurring as a result of this wave of potential change will necessarily have a distributed range of lifetimes. This capacitance change may be described as trap filling, but it may also be distinguished from the recombination reaction, a distinction not made in a statistical model. By use of the current measurement accompanying the cation decay, it is possible to deconvolve the porous electrode charging from the recombination reaction. The recombination reaction, when taken separately, is directly proportional to surface charge.

Conclusions

The active ions, Li^+ or Ca^{2+}, shorten the dye cation lifetime, while an inert ion, TBA^+, does not. In the absence of an applied bias, the cation decays are the same, within experimental error, for electrolytes containing Li^+ or Ca^{2+} ions. When a negative bias is applied, the rate of the recombination reaction is faster with Ca^{2+} than with Li^+ present, suggesting that the density of surface charge is a factor in the recombination reaction rate.

Li^+ ions in the electrolyte do not change the rate of charge recombination on sensitized ZnO films. Active ions change the oxidation state of the TiO_2, which populates the lowest energies in the conduction band, creating a surface dipole and lowering the work function.

Water, as low as 350 ppm, increases the rate of recombination in sensitized TiO_2 films in inert electrolyte at -400 mV and more negative, and on the order of 1000 ppm, it causes the N719 dye to desorb. Water inhibits the effect of Li^+ on TiO_2 but does not change the magnitude of the current, as it does in the TBA^+ and Ca^{2+} systems. If Li^+ is not present, then the interaction of holes with OH^- sites may produce a hole current that enhances the electronic current.

Applying a bias to sensitized TiO_2 in an inert electrolyte causes the electrode to become more resistive with more negative applied biases. However, sensitized TiO_2 immersed in an electrolyte containing active ions becomes less resistive with more negative applied biases.

The current results from (i) Helmholtz layer charging, (ii) porous electrode charging, (iii) the recombination reaction, and (iv) surface diffusion of the ions.

The recombination half-life is directly proportional to the amount of ions deposited on the electrode. The literature suggests that the quantity of adsorbed ions is equal to the population of electrons in the energy band of the five-coordinated titaniums. If this is so, then the recombination reaction is first-order in the concentration of electrons in this energy band.

Acknowledgment. The author is especially grateful to Jenny Nelson for her supervision, James Durrant for his guidance, Sven Södergren for indispensable advice, and Greenpeace Environmental Trust and Overseas Research Scholarships for financial support.

References and Notes

(1) O'Regan, B.; Grätzel, M. *Nature* **1991**, *353*.

(2) Nazeeruddin, M. K.; Kay, A.; Rodicio, I.; Humphrey-Baker, R.; Muller, E.; Liska, P.; Vlachopoulos, N.; Gratzel, M. *J. Am. Chem. Soc.* **1993**, *115*, 6382.

(3) Barbé, C. J.; Arendse, F.; Comte, P.; Jirousek, M.; Lenzmann, F.; Shklover, V.; Grätzel, M. *J. Am. Ceram. Soc.* **1997**, *80*, 3157.

(4) Tachibana, Y.; Moser, J.; Gratzel, M.; Klug, D. R.; Durrant, J. R. *J. Phys. Chem.* **1996**, *100*, 20056.

(5) Hannappel, T.; Burfeindt, B.; Storck, W.; Willig, F. *J. Phys. Chem. B* **1997**, *101*, 6799.

(6) Heimer, T. A.; Heilweil, E. J. *J. Phys. Chem. B* **1997**, *101*, 10990.

(7) Ellingson, R. J.; Asbury, J. B.; Ferrere, S.; Ghosh, H. N.; Sprague, J. R.; Lian, T.; Nozik, A. J. *J. Phys. Chem. B* **1997**, *101*, 6455.

(8) Haque, S. A.; Tachibana, Y.; Willis, R. L.; Moser, J.; Gratzel, M.; Klug, D. R.; Durrant, J. R. *J. Phys. Chem. B* **2000**, *104*, 538.

(9) Haque, S. A.; Tachibana, Y.; Klug, D. R.; Durrant, J. R. *J. Phys. Chem. B* **1998**, *102*, 1745.

(10) Kelly, C. A.; Farzad, F.; Thompson, D. W.; Stipkala, J. M.; Meyer, G. J. *Langmuir* **1999**, *15*, 7047.

(11) Kelly, C. A.; Meyer, G. J. *Coord. Chem. Rev.* **2001**, *211*, 295.

(12) Heimer, T. A.; Heilweil, E. J.; Bignozzi, C. A.; Meyer, G. J. *J. Phys. Chem. A* **2000**, *104*, 4256.

(13) Kuciauskas, D.; Freund, M. S.; Gray, H. B.; Winkler, J. R.; Lewis, N. S. *J. Phys. Chem. B* **2001**, *105*, 392.

(14) Hasselmann, G. M.; Meyer, G. J. *J. Phys. Chem. B* **1999**, *103*, 7671.

(15) Tachibana, Y.; Haque, S. A.; Mercer, I. P.; Klug, D. R.; Durrant, J. R. *J. Phys. Chem. B* **2000**, *104*, 1198.

(16) Diebold, U. *Surf. Sci. Rep.* **2003**, *48*, 53.

(17) Willis, R. L.; Olson, C.; O'Regan, B.; Lutz, T.; Nelson, J.; Durrant, J. R. *J. Phys. Chem. B* **2002**.

(18) Zakeeruddin, S. M.; Nazeeruddin, M. K.; Pechy, P.; Rotzinger, F. P.; Humphrey-Baker, R.; Kalyanasundarum, K.; Gratzel, M.; Shklover, V.; Haibach, T. *Inorg. Chem.* **1997**, *36*, 5937.

(19) Rensmo, H. *J. Chem. Phys.* **1999**, *111*, 2744.

(20) Bredow, T.; Apra, E.; Catti, M.; Pacchioni, G. *Surf. Sci.* **1998**, *418*, 150.

(21) Brause, M.; Skordas, S.; Kempter, V. *Surf. Sci.* **2000**, *445*, 224.

(22) Casanova, R.; Prabhakaran, K.; Thornton, G. *J. Phys.: Condens. Matter* **1991**, *3*, S91.

(23) Grant, A. W.; Campbell, C. T. *Phys. Rev. B* **1997**, *55*, 1844.

(24) Muscat, J.; Harrison, N. M.; Thornton, G. *Phys. Rev. B* **1999**, *59*, 15457.

(25) Szczepankiewicz, S. H.; Moss, J. A.; Hoffman, M. R. *J. Phys. Chem. B* **2002**, *106*, 7654.

(26) Henrich, V. E.; Cox, P. A. *The Surface Science of Metal Oxides*; University Press: Cambridge, U. K., 1994.

(27) de Levie, R. *Electrochim. Acta* **1963**, *8*, 751.

(28) Posey, F. A.; Morozumi, T. *J. Electrochem. Soc.* **1966**, *113*, 176.

(29) Olson, C. L.; Ballard, I. Charge accumulation and polarization in TiO_2 electrodes, in press.

(30) Solbrand, A.; Lindstrom, H.; Rensmo, H.; Hagfeldt, A.; Lindquist, S.-E. *J. Phys. Chem. B* **1997**, *101*, 2514.

(31) Solbrand, A.; Henningsson, A.; Södergren, S.; Lindstrom, H.; Hagfeldt, A.; Lindquist, S.-E. *J. Phys. Chem. B* **1999**, *103*, 1078.

(32) Crank, J. *The Mathematics of Diffusion*; Clarendon Press: Oxford, U. K., 1956.

(33) Thomas, A. G.; Flavell, W. R.; Kumarasinghe, A. R.; Mallick, A. K.; Tsoutsou, D.; Smith, G. C.; Stockbauer, R.; Patel, S.; Gratzel, M.; Hengerer, R. *Phys. Rev. B* **2003**, *67*, 035110.

(34) Mackrodt, W. C.; Simson, E. A.; Harrison, N. M. *Surf. Sci.* **1997**, *384*, 192.

(35) Smirnov, M.; Baddour-Hadjean, R. *J. Chem. Phys.* **2004**, *121*, 2348.

(36) Wagemaker, M.; Kentgens, A. P. M.; Mulder, F. M. *Nature* **2002**, *418*, 397.

(37) Qu, P.; Meyer, G. J. *Langmuir* **2001**, *17*, 6720.

(38) Södergren, S.; Siegbahn, H.; Rensmo, H.; Lindström, H.; Hagfeldt, A.; Lindquist, S.-E. *J. Phys. Chem. B* **1997**, *101*, 3087.

(39) Augustsson, A.; Henningsson, A.; Butorin, S. M.; Siegbahn, H.; Nordgren, J. *J. Chem. Phys.* **2003**, *119*, 3983.

(40) Krishok, S.; Hofft, O.; Gunster, J.; Stultz, J.; Goodman, D. W.; Kempter, V. *Surf. Sci.* **2001**, *495*, 8.

(41) Krishok, S.; Hofft, O.; Kempter, V. *Surf. Sci.* **2002**, *507*−*510*, 69.

(42) Krishok, S.; Schaefer, J. A.; Höfft, O.; Kempter, V. *Surf. Interface Anal.* **2004**, *36*, 83.

(43) Nelson, J.; Haque, S. A.; Klug, D. R.; Durrant, J. R. *Phys. Rev. B* **2001**, *63*, 205321.